J. Fluid Mech. (1993), *vol.* 253, *pp.* 643–661

Copyright © 1993 Cambridge University Press

A study of turbulent vortices in the near wake of a cylinder

By Y. ZHOU AND R. A. ANTONIA
Department of Mechanical Engineering, University of Newcastle, NSW 2308, Australia

(Received 5 February 1992 and in revised form 4 January 1993)

Turbulent vortices in the wake of a circular cylinder have been examined in some detail following their detection by a method based on vorticity concentration and circulation. The experimental data were obtained at a Reynolds number $Re = 5600$ (based on the free-stream velocity and cylinder diameter) with an array of eight X-wires aligned in the plane of mean shear. Distributions of conditionally averaged vorticity and circumferential velocity within vortices are in reasonable agreement with those inferred from an Oseen vortex. The conditionally averaged streamwise velocity distribution through the vortex centre has a maximum at the centre, implying a vortex convection velocity greater than the local mean velocity. An Oseen vortex model reproduces the measured mean velocity and Reynolds stresses reasonably well. Results are also given for the streamwise variations of vorticity concentration, circulation and size of the vortices.

1. Introduction

The study of organized aspects of the motion in turbulent shear flows has invariably focused attention on the vortical structure of these flows. In particular, the relatively strong organization in the near wake of a cylinder has attracted a great deal of interest (e.g. Davies, 1976; Cantwell & Coles 1983; Kiya & Matsumura 1985; Hussain & Hayakawa 1987; Antonia 1991). While these investigations have yielded useful information about the topology of the organized motion and the mechanism for turbulence production, little is known about the velocity and vorticity distributions of turbulent vortices. Such information, as well as knowledge of the streamwise and transverse locations of the vortices, is important in the development of vortex models for this and other flows. For example, an Oseen-type vortex model, together with the measured spatial arrangement of vortices, was recently used by Bisset, Antonia & Browne (1990) to calculate the mean velocity and Reynolds stresses in the far wake of a cylinder. The velocity and vorticity distributions for an Oseen vortex have been approximately verified for a laminar wake (see § 2). Such verification is generally lacking in the turbulent case although Robinson (1991) has shown, using direct numerical simulations of a turbulent boundary layer, that at least some quasi-streamwise vortices near the wall resemble Oseen vortices.

The main aims of the present study are: (i) to provide data on the velocity and vorticity distributions within turbulent vortices, and (ii) to investigate an appropriate kinematic model for this flow. A number of other issues are also addressed, for example the spatial arrangement, streamwise evolution and possible interactions associated with an array of vortices.

2. Velocity and vorticity distributions within a vortex: a brief review

The Oseen vortex is an exact non-steady solution to the Navier–Stokes equations. The circumferential velocity v_θ is given by (e.g. Granger, 1985, p. 475)

$$v_\theta = \frac{\Gamma_0}{2\pi r}\left[1-\exp\left(-\frac{r^2}{4\nu t}\right)\right], \tag{1}$$

where r is the radius (origin at vortex centre), ν is the kinematic viscosity and Γ_0 is the vortex strength, defined as the circulation at time $t = 0$ (i.e. when viscosity first becomes important). For $t > 0$, (1) may be rewritten as

$$v_\theta = \frac{\Gamma_0}{2\pi r}\left[1-\exp\left(-1.26\frac{r^2}{r_1^2}\right)\right], \tag{2}$$

where r_1 is the value of r at which v_0 is maximum; r_1 may be loosely identified with the core of the vortex. Since the radial velocity v_r is zero, the vorticity is given by

$$\omega = \frac{\partial v_\theta}{\partial r}-\frac{1}{r}\frac{\partial v_r}{\partial \theta}+\frac{v_\theta}{r} = \omega_0 \exp\left(-1.26\frac{r^2}{r_1^2}\right), \tag{3}$$

where $\omega_0 = 1.26\,\Gamma_0/\pi r_1^2$.

Equations (1), (2) and (3) have been verified experimentally for laminar vortices. For example, using the Oseen vortex as the basic building block, Schaefer & Eskinazi (1959) calculated the velocity distribution for a vortex street model which agreed with their experimental results in a laminar wake ($Re = 62$). Similar verifications were reported ($Re = 140$) by Okude & Matsui (1987) who used both hot-wire and visualization techniques and by Green & Gerrard (1991) ($Re = 80$) using optical interferometry. Using hot wires, Okude & Matsui (1990) measured the vorticity distribution in a cylinder wake ($Re = 140$) and found it to be in reasonable agreement with (3).

A number of models have been used to match, at least kinematically, experimental and numerical data in several different turbulent flows (e.g. Bloor & Gerrard 1966; Davies 1976; Oler & Goldschmidt 1982; Bisset *et al.* 1990; Robinson 1991). The Oseen vortex and the model proposed by Hoffmann & Joubert (1963) are two such examples. Hoffmann & Joubert suggested, using dimensional arguments and Prandtl's mixing-length theory, that for the inner core of turbulent vortices $v_\theta \propto r$, while for the outer core $v_\theta \propto r^{-1}\ln r$. A similar model was also suggested by Saffman (1973).

In their investigation of vortex strength and velocity distribution in a cylinder wake ($Re = 2\times10^3$ and 1.6×10^4), Bloor & Gerrard (1966) found that Hoffmann & Joubert's model was valid except for the inner core region, where they concluded, indirectly, that the Oseen vortex was more appropriate. The latter model is used more frequently. For example, it was used by Davies (1976) to model the planar near wake of a D-shape cylinder, by Oler & Goldschmidt (1982) to model the self-preserving region of a plane jet, and by Bisset *et al.* (1990) to model the self-preserving far wake of a circular cylinder. In general, this model can lead to a mean velocity distribution that is in accord with the measurements but does not yield a satisfactory shear stress distribution. For example, Oler & Goldschmidt obtained a shear stress of sign opposite to that measured. Bisset *et al.* needed to introduce a phase shift between velocity components to calculate the shear stress correctly. The difficulty experienced may be partly due to the complexity of turbulent flows and partly to the lack of information on individual turbulent vortices. In this paper, we attempt to provide such information and use it to develop a kinematic model that mimics the measured near-wake distributions of mean velocity and Reynolds stresses.

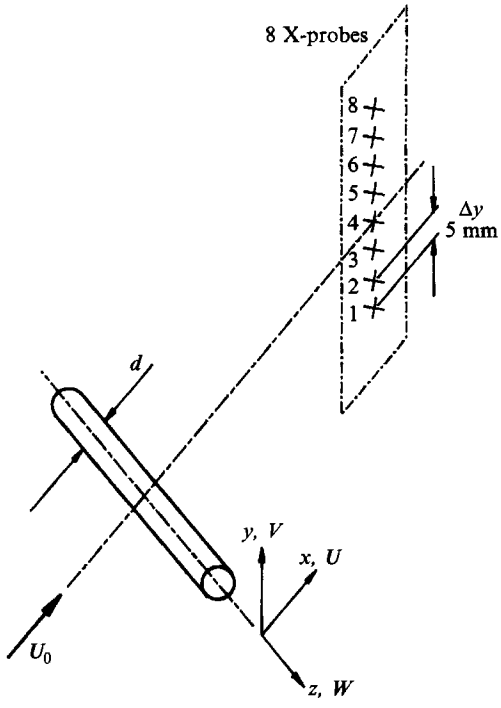

FIGURE 1. Schematic experimental arrangement.

3. Experimental details

Experiments were carried out in an open-return low-turbulence wind tunnel with a 2.4 m long working section (0.35 m × 0.35 m). The bottom wall could be tilted to achieve a zero streamwise pressure gradient. A circular cylinder ($d = 12.5$ mm) made of stainless steel rod was installed in the midplane and across the width of the working section, 20 cm from the exit plane of the contraction, to generate the wake. This resulted in a blockage of about 3.6%. Measurements were made at a constant free-stream velocity ($U_0 = 6.7$ m/s) in the range $10 \leqslant x/d \leqslant 60$. The corresponding Reynolds number Re was 5600. In the free stream the longitudinal and lateral turbulence intensities were about 0.05% and 0.08% respectively. At the centreline, the longitudinal turbulence integral lengthscale was estimated to be equal to about $0.3d$.

A rake of eight X-probes (the spacing between adjacent probes was about 5 mm) was aligned transversely, with probe 4 on the centreline (figure 1), to measure velocity fluctuations u and v at the eight X-probe locations. The Wollaston (Pt–10% Rh) wires, 5 μm in diameter and an etched length of about 1.3 mm, were operated with constant-temperature circuits. The signals were offset, amplified and then digitized using a 16 channel, 12 bit data acquisition system, at a sampling frequency of 3 kHz per channel. The vortex shedding frequency f_s as inferred from the main peak in the v-spectrum was equal to 110 Hz. Using velocity and yaw calibrations, signals proportional to u and v were formed and stored on digital tapes. A record duration of about 30 s was used.

The mean velocity $\bar{U}$, was obtained at each X-probe location using a personal computer and a data-logging system. U_0 was monitored continuously with a Pitot static tube connected to a Baratron pressure transducer.

4. Vortex Detection Method

A wide variety of methods have been used for detecting the organized motion in the wake of a circular cylinder (e.g. Cantwell & Coles 1983; Kiya & Matsumura 1985; Hussain & Hayakawa 1987; Antonia 1991). Although each method has focused on different aspects of the organized motion, results from these different methods are basically in agreement with each other, due in no small part to the distinct organization of this flow. As the present focus is directed mainly at determining the characteristics of vortices, it seems important that the detection method should generally focus on vorticity. A method similar to that of Hussain & Hayakawa is therefore adopted. It is also important to minimize the smearing of vortex locations so that the details of individual vortices can be extracted unambiguously. This requires criteria additional to the vorticity concentration since a strong vorticity concentration is not necessarily associated with large-scale vortices and may be due to some secondary vortices (e.g. Wei & Smith 1986) that are not of direct interest here. Hussain & Hayakawa specified the size of vortices by requiring the streamwise and transverse extents of the smoothed vorticity to exceed a certain threshold value. In the present detection, circulation is used as an additional criterion. Details of the detection method are given below.

There is little doubt that turbulent vortices are three-dimensional. While information on the three components of vorticity and the pressure field would be desirable for detecting the vortices, this is not practical in an experimental context. In the present scheme, only an approximation to the spanwise vorticity is used, namely

$$\omega = \frac{\Delta V}{\Delta x} - \frac{\Delta U}{\Delta y}, \tag{4}$$

where $\Delta x = -\Delta t U_c$ and Δy is the spacing between adjacent X-probes. In (4) the instantaneous signals U and V are formed by adding the local mean velocity values of $\bar{U}$ and $\bar{V}$ (≈ 0) to the digital time series of the fluctuations u and v, i.e. $U \equiv \bar{U}+u$ and $V \equiv \bar{V}+v$. Note that the average convection velocity U_c of the vortex has been used in Taylor's hypothesis for converting the time separation Δt into a streamwise distance. The values of U_c, obtained by various methods, increase from about $0.85U_0$ to $0.92U_0$ as x/d increases from 10 to 60. Details associated with the determination of U_c are given in Zhou & Antonia (1992*a*).

Considering the coarse spacing ($\Delta y \approx 5$ mm) between probes, two extra rows of vorticity data points are interpolated between each pair of existing rows by least-square-fitting bi-cubic spline functions to the vorticity data obtained with (4). Some of the interpolated points are examined to ensure that the interpolation is reasonable.

The criterion used for initially detecting a vortex and locating its centre is

$$|\omega_p| > k_\omega S_m, \tag{5}$$

where ω_p is a peak value of vorticity, $S_m = (\partial \bar{U}/\partial y)_{max}$ is the local maximum mean shear, and k_ω is a threshold, at first chosen arbitrarily and later modified after visually examining the detection locations on contour plots of the instantaneous spanwise vorticity. Since ω_p is a local quantity, the local maximum mean shear appears to be a logical choice in (5). One advantage in using the vorticity concentration to locate vortices is that vorticity should not be affected by the choice of U_c. Although Taylor's hypothesis, $\Delta x = -U_c \Delta t$, is invoked in (4), the convection velocity varies only slightly across the wake (Zhou & Antonia 1992*a*) so that the influence on the detection locations is only small.

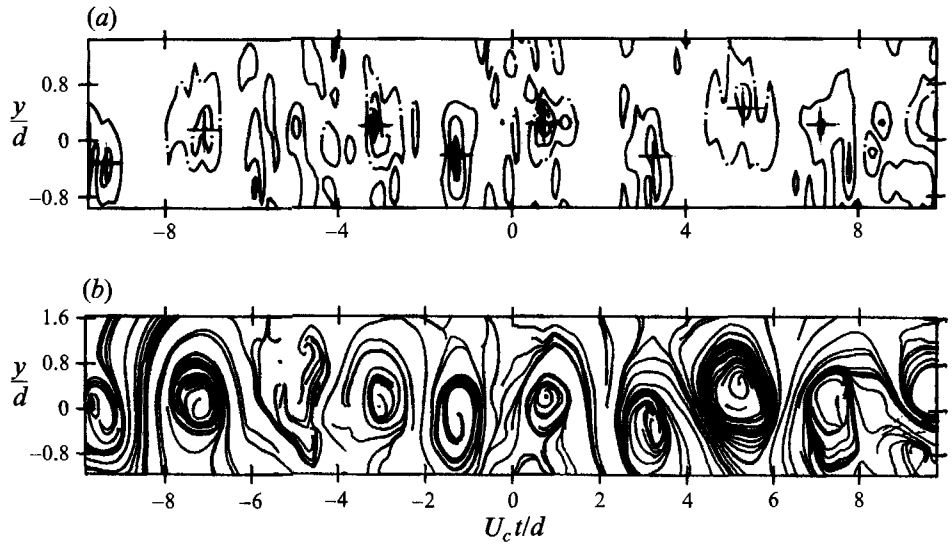

FIGURE 2. Examples of detections (indicated by +) at $x/d = 10$ on (*a*) instantaneous vorticity contours (solid and dashed lines represent positive and negative contours respectively) and (*b*) sectional streamlines observed in a moving frame of reference ($\bar{U}_c/U_0 = 0.87$). $t = 0$ is arbitrary.

Before the circulation can be determined, an analytical expression for $\omega(r, \theta)$ is needed. A surface-fit, using fourth-order Chebychev series, is applied to an approximately square grid of vorticity data centred on ω_p. The origin of the cylindrical coordinates (r, θ) is at the location of ω_p.

To eliminate the dependence of ω on θ and to estimate the vortex size, the mean vorticity at a radius r from the vortex centre is defined by

$$\Omega(r) = \frac{1}{2\pi}\int_0^{2\pi} \omega(r, \theta)\,\mathrm{d}\theta, \quad 0 \leqslant r \leqslant r_m, \tag{6}$$

where r_m is half the total size of the grid.

The vortex size is then estimated as the value of r_v for which

$$|\Omega(r_v)| = \Omega_c, \tag{7}$$

where Ω_c is an assumed minimum vorticity level for vortices. While the choice of Ω_c affects the value of r_v, it does not affect the vortex detection. Here, Ω_c is chosen to be $1.5S_m$, following Hussain & Hayakawa's observation that the maximum circumferential velocity around the vortex centre occurs when $\omega \approx S_m$. It is shown in §5 that $\Omega_c = 1.5S_m$ is a reasonable choice for the vortex core radius.

Equation (7) is solved for r_v by using a quasi-Newton optimizing algorithm (Gill & Murray 1976) which searches for the minimum of $[|\Omega(r)| - \Omega_c]^2$ $(0 \leqslant r \leqslant r_m)$. Once r_v is determined, the corresponding circulation

$$\Gamma = 2\pi \int_0^{r_v} \Omega(r)\, r\,\mathrm{d}r \tag{8}$$

may be calculated. Since the detection aims to educe large-scale vortices, the magnitude of Γ is required to satisfy the following condition:

$$|\Gamma| \geqslant k_\Gamma S_m d^2, \tag{9}$$

where k_T is a threshold determined in similar fashion to k_ω. The final values of k_ω and k_T are chosen separately and fall between about 4.0 and 8.0 or 0.5 and 0.6 depending on the value of x/d.

Several vorticity peaks may be associated with one vortex; an example is seen in figure 2(*a*), where more than one peak appears in the range $7 < tU_c/d < 9$ and they are obviously related to the same vortex (this is clearer in the sectional streamlines of figure 2(*b*); these streamlines are constructed using the procedure outlined in Bisset *et al.* 1990). To avoid detecting such spurious vorticity peaks, another condition was added; a maximum of one detection is made within half an average vortex shedding period for vortices of the same sign.

Detection locations seemed quite reasonable when viewed on plots of vorticity contours and sectional streamlines, e.g. figures 2(*a*) and 2(*b*). In figure 2(*a*) some vorticity concentrations (e.g. $7 < tU_c/d < 9$) of either sign are not detected. This is either because (5) and (9) are not satisfied or because their peaks lie within half an average shedding period of a detection with a higher value of ω_p (and are therefore ignored).

5. Results

5.1. *Conditional averages*

A few results in this section are presented in the form of conditional averages. (Unless otherwise stated, these are based on negative-vorticity detections.) The conditional average of a quantity F is defined by

$$\langle F\rangle(x',y') = \frac{1}{N}\sum F(x',y'), \tag{10}$$

where the origin of the coordinate system (x',y') is at the detected vortex centre, and N is the total number of detections. $\langle F\rangle$ allows the focus to be on the coherent motion of the vortex. When cylindrical coordinates are used, with the vortex centre at $r = 0$, $\langle F\rangle$ may be written

$$\langle F\rangle(r) = \frac{1}{N}\sum F(r), \tag{11}$$

the dependence on θ having been eliminated, as discussed in §4.

5.2. *Detection frequency*

The dependence on x/d of the average non-dimensional detection frequency $(N/T)\,d/U_0$ is shown in figure 3, where T is the overall duration. This figure provides some information on the rate at which vortices decay, with the caveat that for $x/d \geqslant 30$ some vortices may be outside the range of the rake and therefore escape detection. At $x/d = 10$, $(N/T)\,d/U_0$ is about 0.2. This value is within the expected shedding frequency range of $f_s\,d/U_0 = 0.20$–0.21 (Roshko 1954), indicating that nearly all vortices are detected.

5.3. *Vorticity*

The probability density function of ω_p, denoted by $p_{\omega_p}(\equiv P/\Delta\omega_p$, where P is the probability that ω_p is in the range ω_p to $\omega_p+\Delta\omega_p)$, is shown in figure 4 for $x/d = 10$. (Similar distributions have been obtained at other values of x/d.) The distributions of p_{ω_p} indicate that there is a considerable spread in ω_p, ranging from about $5S_m$ to about $19S_m$, the mode occurring at about $9.5S_m$. As vortices travel downstream, their vorticity level declines gradually (figure 5).

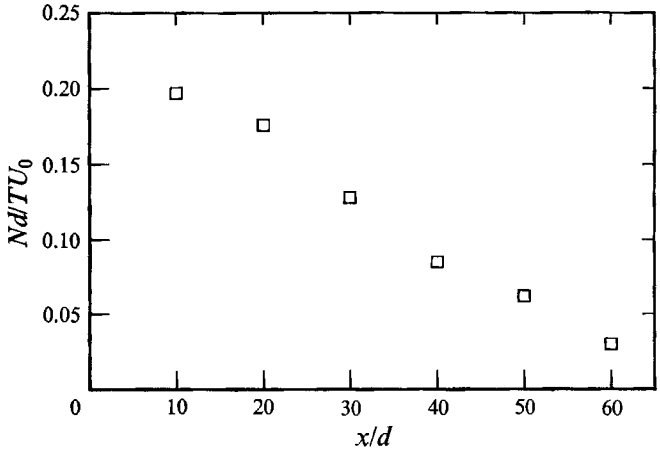

FIGURE 3. Streamwise variation of vortex detection frequency.

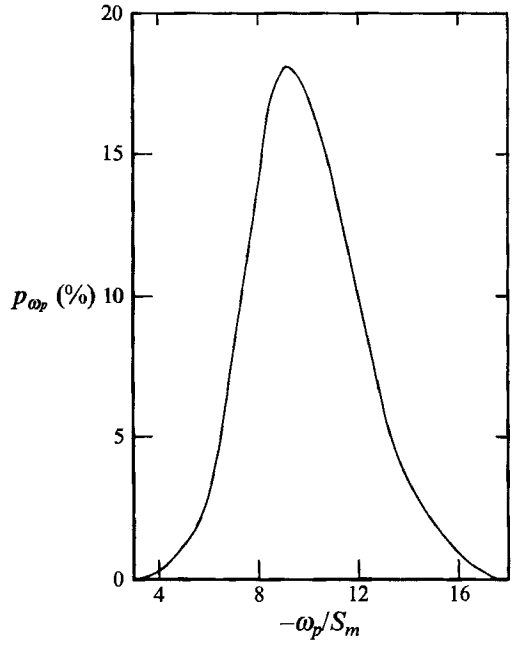

FIGURE 4. Probability density function of peak vorticity at $x/d = 10$. ($k_\omega = 4.0$).

The vorticity distribution within an individual vortex is investigated using $\langle\Omega\rangle(r)$, the conditional mean vorticity at a radius r from the vortex centre, and $\langle\omega\rangle(x', 0)$, the conditional vorticity in a longitudinal direction through the vortex centre. Figure 6 shows that $\langle\Omega\rangle(r)/\Omega_0$, where $\Omega_0 \equiv \langle\Omega\rangle(0)$, is almost universal for $10 \leqslant x/d \leqslant 60$ and reasonably well fitted by an exponential curve

$$\frac{\langle\Omega\rangle(r)}{\Omega_0} = \exp\left[-1.26\left(\frac{r}{0.52d}\right)^2\right]. \tag{12}$$

This is closely similar to (3), with $r_1 = 0.52d$. A similar behaviour is observed for $\langle\omega\rangle(x', 0)/\omega_0$ (figure 6), where $\omega_0 \equiv \langle\omega\rangle(0, 0)$, which partly justifies the use of $\Omega(r)$

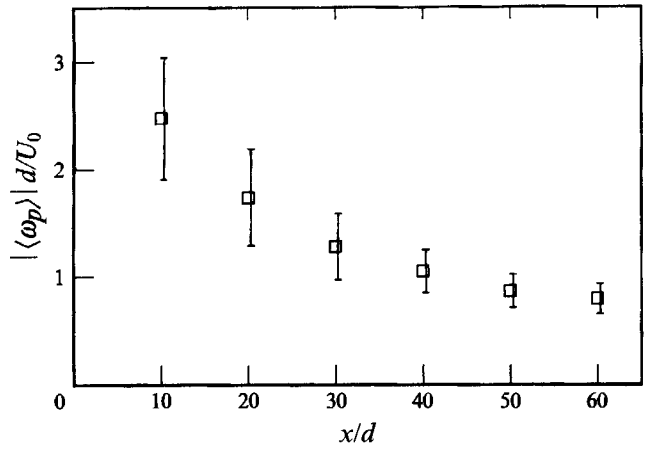

FIGURE 5. Streamwise variation of peak vorticity. The error bar denotes ± standard deviation.

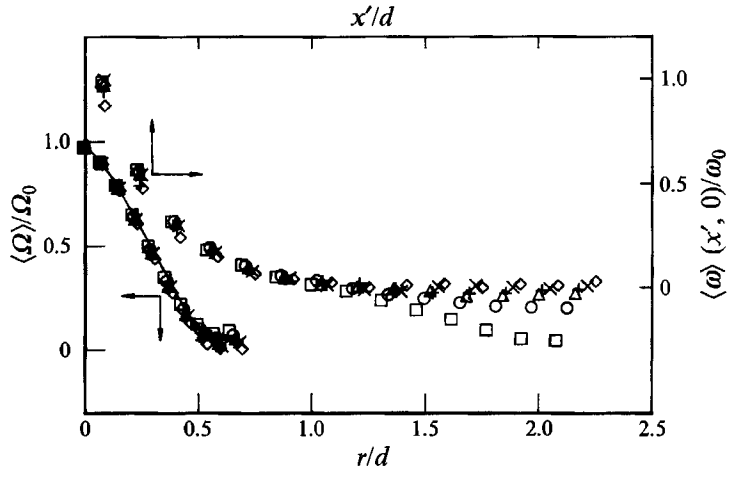

FIGURE 6. Conditional vorticity distributions of $\langle\omega\rangle(x',0)$ in the x-direction through the vortex centre and $\langle\Omega\rangle(r)$ in the radial direction: □, $x/d = 10$; ○, 20; △, 30; +, 40; ×, 50; ◇, 60; ——, $\exp[-1.26(r/0.52d)^2]$.

for representing the radial distribution of vorticity. However, the magnitude of $\langle\omega\rangle(x',0)/\omega_0$ decreases slightly more rapidly near the centre than $\langle\Omega\rangle(r)/\Omega_0$. This is probably attributable to the relatively large uncertainty (±2.5 mm) in the lateral location of vortices (the uncertainty in the streamwise location is only about ±1 mm, i.e. $\pm\frac{1}{2}U_c$/sampling frequency) which may result in the detected vortex centre ($x' = y' = 0$) being slightly displaced from the actual centre. If an ideal two-dimensional vortex has an axisymmetric vorticity which decreases monotonically in a radial direction away from a central extremum (e.g. McWilliams 1990), any vorticity distribution (normalized by its maximum) along a line which does not pass through the vortex centre will indicate a reduced spread or a more rapid decrease as the distance from the centre increases. It is possible that the spread of $\langle\omega\rangle(x',0)/\omega_0$ may have been more affected by the uncertainty in the lateral location of vortex centres than that of $\langle\Omega\rangle(r)/\Omega_0$. The relatively large uncertainty in the lateral location of the vortices can

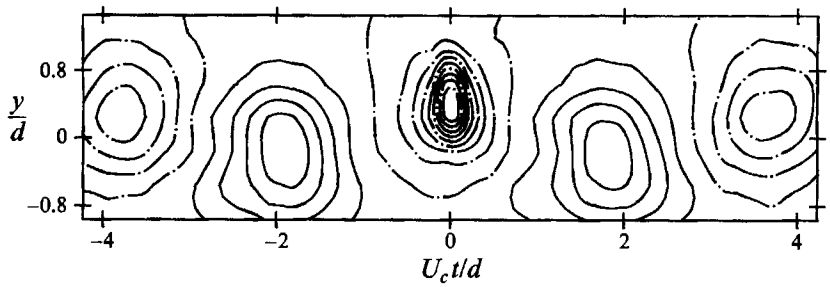

FIGURE 7. Contours of conditional vorticity $\langle\omega\rangle d/U_0$ at $x/d = 10$ based on detections between probes 4 and 5: -1.7 to $+0.7$ (step = 0.2). Solid and dashed lines represent positive and negative contours respectively.

also lead to a lateral elongation of the conditional vorticity contours. This is verified in figure 7 where $\langle\omega\rangle$ is based on the detections between probes 4 and 5. (The same scale has been used for both x- and y-directions.) The contours (not shown here) of $\langle\omega\rangle$, which are based on overall detections, are considerably more stretched than those in figure 7 because of the larger uncertainty in the lateral locations.

The present vorticity distribution is consistent with that observed in McWilliams' (1990) numerical simulations. For individual vortices, McWilliams found that vorticity had an approximately Gaussian distribution, independent of time (after an initial short period) if normalized by its extremum, and attributed this behaviour to viscous diffusion.

5.4. *Velocity distribution*

The departure of the instantaneous velocity (U, V) from its value (U_c, V_c) at a vortex centre (x_c, y_c) is given by

$$u'(x', y') = U(x', y') - U_c, \tag{13}$$

$$v'(x', y') = V(x', y') - V_c. \tag{14}$$

The conditional lateral and longitudinal velocities at $y' = 0$, i.e. $\langle v'\rangle(x', 0)$ and $\langle u'\rangle(x', 0)$ (for simplicity written as $\langle v'\rangle$ and $\langle u'\rangle$ hereafter), are shown in figure 8. In the context of comparing velocity distributions between the turbulent vortex and the Oseen vortex $\langle v'\rangle$ may be identified with the circumferential velocity. The variation of $\langle v'\rangle/U_0$ (figure 8*b*) is similar to that of an Oseen vortex: it increases almost linearly near the centre and reaches a maximum before decreasing slowly. As x/d increases, the magnitude of $\langle v'\rangle/U_0$ decreases.

In contrast to $\langle v'\rangle/U_0$, the magnitude of $\langle u'\rangle/U_0$ (figure 8*a*) is small. One feature of $\langle u'\rangle/U_0$ is that the maximum occurs at the vortex centre. (This has also been verified for positive vortices.) It may also be seen on conditional velocity vectors. As shown in figure 9, the direction of the streamwise velocity component between consecutive vortices tends to be opposite to the flow, as a result of interactions between opposite-signed vortices. This suggests that the convection velocity, or velocity at the vortex centre, must be greater than the local mean velocity, consistent with earlier observations, e.g. Davies (1976) and Zhou & Antonia (1992*a*).

5.5. *Vortex growth*

The change of size of the vortex is investigated by examining both the conditional average $\langle r_v\rangle$ corresponding to $\Omega_c = 1.5S_m$ and the vortex core radius $\langle r_1'\rangle$ corresponding to the measured maximum velocity $\langle v_1'\rangle$. Figure 10 shows that $\langle r_v\rangle$ and

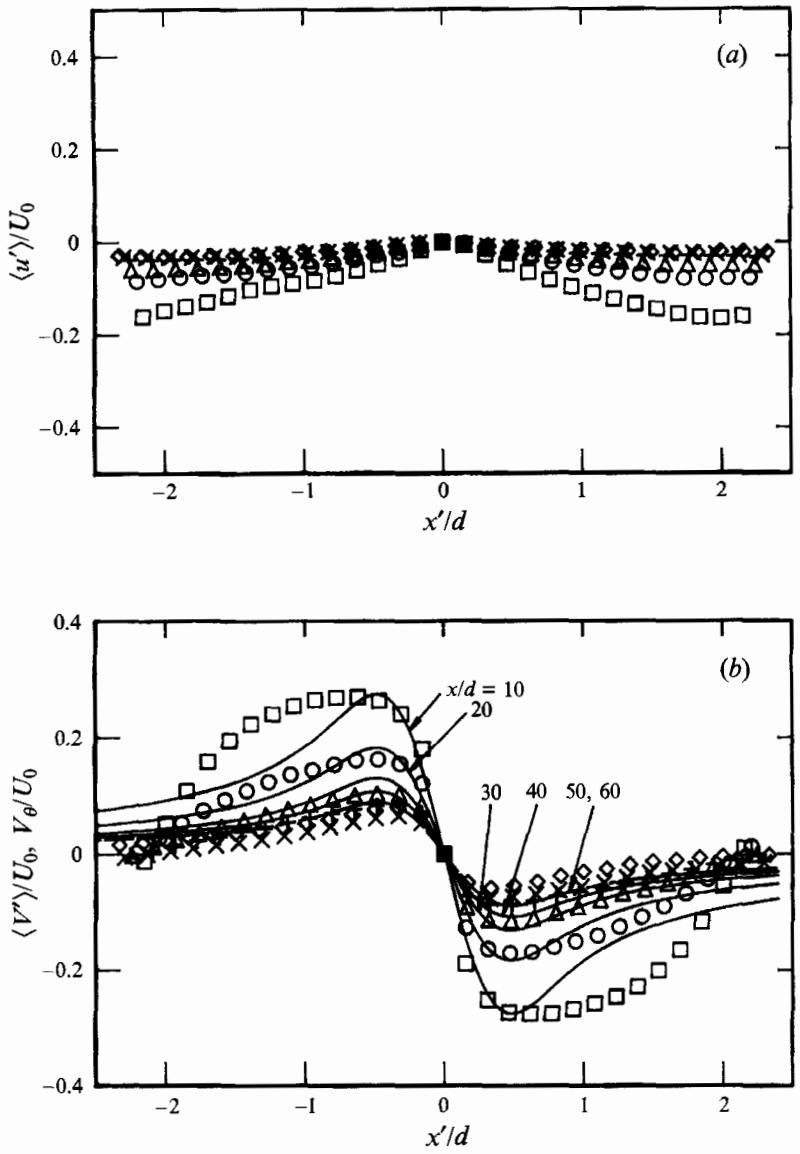

FIGURE 8. Conditional velocity distributions in the x-direction through the vortex centre. (*a*) Longitudinal velocity; (*b*) lateral velocity and calculated circumferential velocity: □, $x/d = 10$; ○, 20; △, 30; +, 40; ×, 50; ◇, 60; ——, calculation.

$\langle r_1' \rangle$ are in reasonable agreement with each other, which corroborates the choice of Ω_c ($\equiv 1.5 S_m$) in §4. Both decrease slowly as x/d increases, suggesting no increase in cross-sectional area of the vortex in the region $10 \leqslant x/d \leqslant 60$. The contour plots of $\langle \omega \rangle / S_m$ at different x/d values (not shown here) exhibit the same trend as $\langle r_v \rangle$ or $\langle r_1' \rangle$. A similar observation was also reported by Hussain & Hayakawa (1987). McWilliams (1990) found little variation in size when studying the history of a single vortex but noticed a steady increase of the average size, which was attributed mainly to vortex pairing.

Vortex growth can be caused by vorticity diffusion and vortex pairing. The latter is unlikely to be important in a wake (e.g. Cimbala, Nagib & Roshko 1988; Zhou &

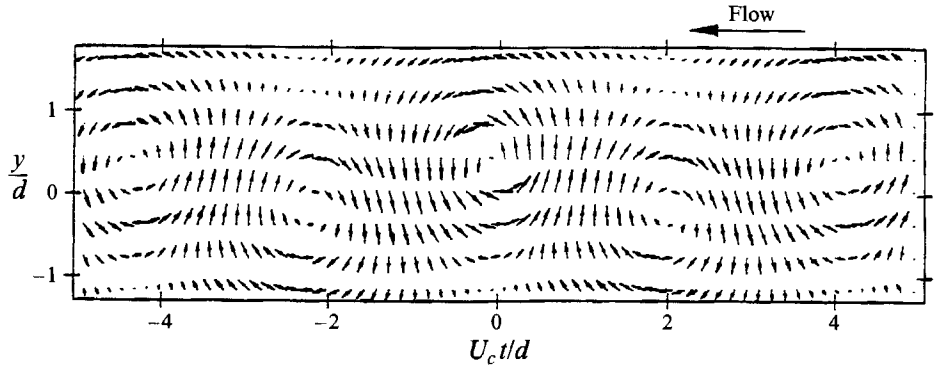

FIGURE 9.Conditional velocity vectors in a moving frame of reference ($U_c/U_0 = 0.87$, $x/d = 10$).

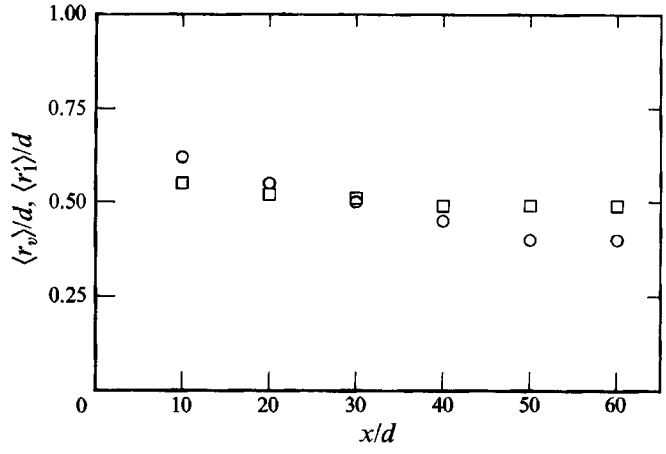

FIGURE 10. Streamwise variation of vortex core radii $\langle r_v\rangle$ (□) and $\langle r_1'\rangle$ (○).

Antonia 1992*a*). The former seems plausible but may be counteracted by the effects of vorticity decay, cancellation (see §5.6 for details) and the tearing of weak vorticity patches from the periphery of a vortex due to strong strain (e.g. Dritschel 1988). It would appear that vortices in a turbulent wake do not grow in the same manner as in a laminar wake (e.g. Okude & Matsui 1987; Green & Gerrard 1991).

Since the contours of $\langle\omega\rangle$ (figure 7) are calculated using data obtained by (4), they are not affected by the interpolation and surface-fitting procedures that have been applied in calculating quantities such as r_v and Γ (§4). A rough estimate of the uncertainty associated with these procedures may therefore be obtained by comparing the value of $\langle r_v\rangle$ (where $\Omega = 1.5S_m$) with the contour size corresponding to $\langle\omega\rangle = 1.5S_m$. *At* $x/d = 10$, $\langle r_v\rangle = 0.55d$, while the average longitudinal and lateral extents of the contour $\langle\omega\rangle = 1.5S_m$ is about $0.53d$. This suggests that the uncertainty in r_v may be around 4%.

5.6. *Circulation*

The circulation within the vortex core is estimated by $\langle\Gamma\rangle$. Provided the turbulent vortex may be modelled by the Oseen vortex (this is justified in §6), the total circulation or vortex strength $\langle\Gamma\rangle$ can be calculated from (2), namely

$$\langle\Gamma_0\rangle = \frac{\langle\Gamma\rangle}{[1-\exp(-1.26)]} \approx \frac{1}{0.72}\langle\Gamma\rangle.$$

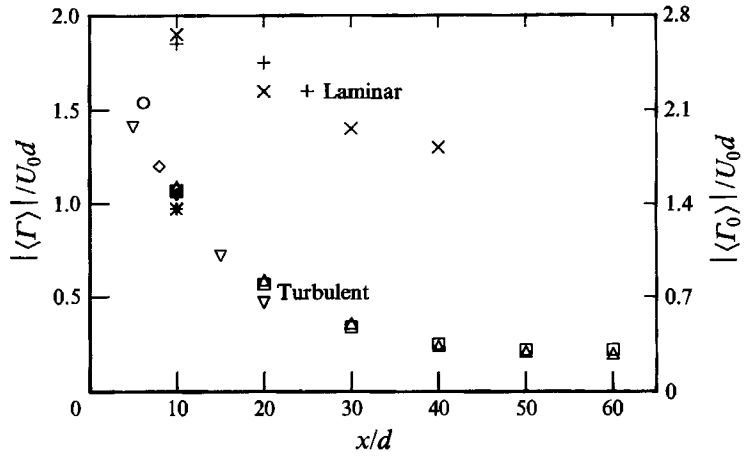

FIGURE 11. Streamwise variation of circulation: □, measured $\langle\Gamma\rangle$ or $\langle\Gamma_0\rangle = 1.4\langle\Gamma\rangle$; △, calculated from the Oseen vortex model; ○, Cantwell & Coles (1983); ◇, Kiya & Matsumura (1985); *, Bloor & Gerrard (1966); ▽, Schmidt & Tilmann (1972); +, Green & Gerrard (1991); ×, Okude & Matsui (1990).

This relation implies that the vortex core contains about 70% of the total circulation.

Figure 11 shows that $\langle\Gamma_0\rangle$, when extrapolated, is in good agreement with the turbulent wake results of Kiya & Matsumura (1985) and Cantwell & Coles (1983) and slightly larger than the results of Bloor & Gerrard (1966) (the largest estimate of Γ_0 in their table 1 is shown in figure 11) and Schmidt & Tilmann (1972) ($Re = 5100$). Relative to the laminar wake results of Okude & Matsui (1990) and Green & Gerrard (1991), $\langle\Gamma_0\rangle$ is much smaller and decreases more rapidly as x/d increases. Green & Gerrard found that vortex cores of opposite-sign vorticity overlapped in a laminar wake. This resulted in a cancellation of vorticity and thus a decline in the vortex strength. For the turbulent wake, this overlap should be more pronounced due to the smaller timescales. This would explain why the vortex strength decays more rapidly in the turbulent wake and would partly account for the lack of growth in the size of the turbulent vortices.

6. Relevance to modelling with an Oseen vortex

In the preceding section, the measured vorticity and circumferential velocity were found to have similar distributions to those of an Oseen vortex. It is appropriate here to assess briefly the relevance of an Oseen vortex to modelling.

The measured vorticity distribution, (12), can be written in similar form to (3), namely

$$\langle\Omega\rangle(r) = \Omega_0 \exp[-1.26(r/r_1)^2], \tag{15}$$

where $r_1 = 0.52d$. If (15) applies to an Oseen vortex, the circumferential velocity v_θ can be calculated from (2) after replacing Γ_0 by $\Omega_0 \pi r_1^2/1.26$. The calculation is generally in good agreement with the measured $\langle v'\rangle$ distributions for $|x'/d| \lesssim 0.6$ (figure 8*b*). A relatively large departure occurs at $x/d = 10$. This does not necessarily invalidate the use of the model since v_θ is calculated from an isolated Oseen vortex, while $\langle v'\rangle$ comprises the combined effect of a sequence of turbulent vortices. At $x/d = 10$, alternating vortices are dominant (Antonia 1991). The lateral motion should therefore be reinforced (Bisset *et al.* 1990), which may explain why $\langle v'\rangle$ is significantly greater

than v_θ when $x'/d > 0.5$. When r_1 is determined, with a value of $0.4d$, from a curve of best fit to $\langle\omega\rangle(x',0)$ (figure 6), v_θ agrees less well with experiment than when using the value of $0.52d$ inferred from $\langle\Omega\rangle(r)$, i.e. (12). A possible reason for this is that $\langle\Omega\rangle(r)$ represents the characteristic distribution of vorticity better than $\langle\omega\rangle(x',0)$. The model circulation within the vortex core is given by $\Gamma = 2\pi r_1 v_\theta(r)$. Figure 11 shows that Γ coincides quite well with $\langle\Gamma\rangle$. The above observations suggest that in a modelling context, the Oseen vortex should be adequate for calculating the vorticity, circulation and circumferential velocity, provided that measured values of Ω_0 and r_1 are used.

7. An Oseen vortex model based on measurement

Using the Oseen vortex as the basic building block, the present model includes as much experimental data as possible, such as the lateral and longitudinal separations, size and strength of the vortices. In contrast, previous models were generally based only partly on measurements, possibly because of a dearth of experimental data. For example, Davies (1976) arrived at the vortex strength Γ_0 and core radius r_1 by matching them to the measured peak vorticity. Oler & Goldschmidt's (1982) model used measured values of the longitudinal spacing and convection velocity of vortices. The lateral spacing Γ_0 and r_1 were governed by similarity relationships and adjusted so that the calculated mean-velocity profiles at $x/d = 30$ agreed with measurement. Bisset *et al.* (1990) used the experimental value for the longitudinal spacing, whilst Γ_0 was arbitrary (all results were normalized) and r_1 was adjusted for best agreement between calculated and measured profiles.

The precise number of vortices in the computational domain is unlikely to be critical, although too small a number would not allow the calculated flow to provide a continuous approximation to the real flow while too large a number would obviously detract from the simplicity of the model. Here, 31 vortices were used in the computational domain, with a further six vortices added beyond each extremity of this domain to avoid end effects. At $x/d = 10$, the relative probability of the duration τ between adjacent vortices of opposite sign (figure 12) exhibits two side lobes at $\tau U_c/d \approx 2.1$ (half the average wavelength) and is nearly zero in the range $-0.7 \lesssim \tau U_c/d \lesssim 0.7$, reflecting the importance of alternating vortices and suggesting the arrangement shown in figure 13. The measured average wavelength ($\lambda = 4.2d$) and average lateral separation ($l = 0.8d$ at $x/d = 10$) of vortices have been used.

Equation (2) and the experimental values of r_1 ($= 0.52d$) and Γ_0 ($= 1.5U_0 d$) are used to determine the circumferential velocity v_θ of each vortex. The longitudinal and lateral velocities induced by a vortex located at (x_c, y_c) are calculated using the relations $v_\theta \sin\theta$ and $v_\theta \cos\theta$, where $\theta = \tan^{-1}[(y-y_c)/(x-x_c)]$. The velocity at any given point is determined by superposing the contributions from all vortices, namely

$$U = U_0 - \frac{1}{n}\sum v_\theta \sin\theta, \quad V = \frac{1}{n}\sum v_\theta \cos\theta \tag{16}$$

where n ($= 43$) is the total number of vortices. The average values $\bar{U}$, $\bar{V}$, $\overline{u^2}$, $\overline{v^2}$ and $\overline{uv}$ are then determined, for example

$$\overline{uv} = \frac{1}{M}\sum_{i=1}^{M}(U_i - \bar{U})(V_i - \bar{V}),$$

where M ($= 400$) is the total number of grid points in the longitudinal direction. $\bar{V}$ is ignored as it is always at least one order of magnitude smaller than $\bar{U}$.

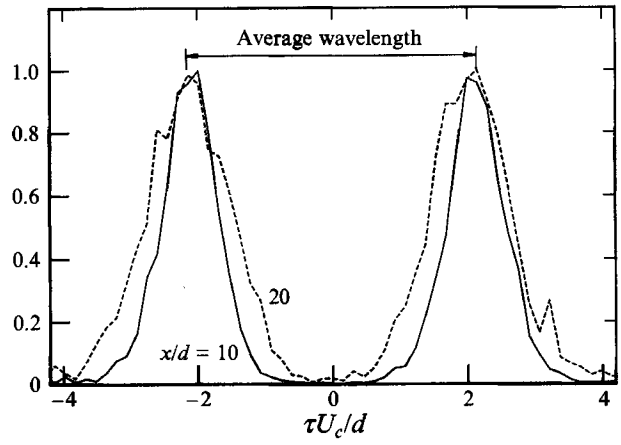

FIGURE 12. Relative probability of duration between adjacent opposite-signed vortices. ($\tau = 0$ is the time at which a negative-signed vortex is detected).

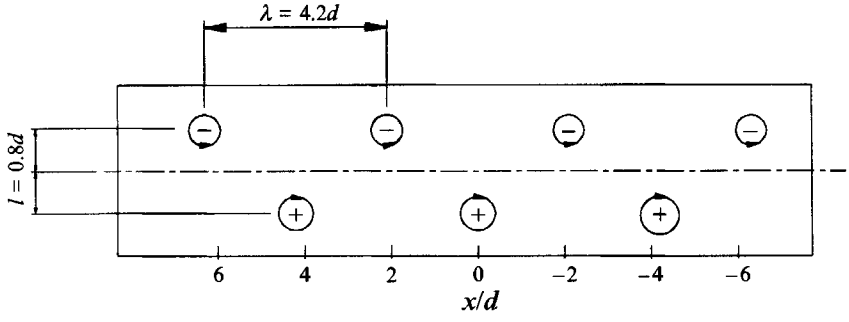

FIGURE 13. Arrangement of vortices in the initial model.

The calculated distributions of $\bar{U}$, $\overline{u^2}$, $\overline{v^2}$ and $\overline{uv}$ are compared in figure 14 with experimental data. These data were obtained in a separate experiment using a three-wire probe (X-wire in combination with a cold wire). While the calculation of $\overline{v^2}$ is in reasonable agreement with the measured distribution, the agreement for $\bar{U}$ and $\overline{u^2}$ is not as good. The calculated values of $\overline{uv}$ are negligible and hence seriously in error.

Clearly some adjustment had to be made to the model to improve its performance. One possibility was to allow the spatial position of the vortices to vary, as observed experimentally, since the arrangement shown in figure 13 was probably too simplistic and did not reflect the possible effect of the variation in the location of vortices on the distributions of $\bar{U}$ and Reynolds stresses. A useful measure of this variation is given by the probability density function p_l† (figure 15) of the lateral separation $l = y_- - y_+$ between opposite-signed vortices, y_- and y_+ denoting the locations of adjacent negative and positive vortices respectively. The mode of p_l occurs at $l = 0.8d$. Note that the value of l can be negative, implying that some positive vortices (generally below the centreline) can sometimes be found above adjacent negative vortices (generally above the centreline) and vice versa. The lateral positions of the vortices in the model were

† Some truncation of this distribution was caused by the array of X-probes not extending to sufficiently large $|y|$. The p_l distribution in figure 15 has been corrected slightly after the lateral distributions of detections obtained from the present data were compared with those obtained in a separate experiment in which all the eight X-probes were on one side of the centreline.

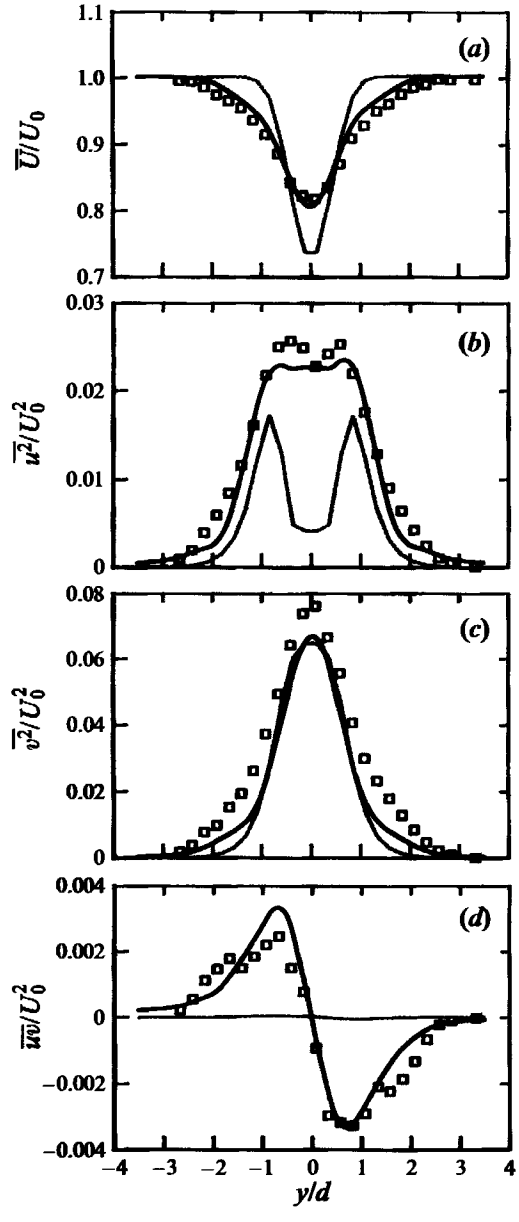

FIGURE 14. Comparison between measurement and calculation: (*a*) mean velocity; (*b*) longitudinal Reynolds normal stress; (*c*) lateral Reynolds normal stress; (*d*) Reynolds shear stress. □, measured conventional average; ——, initial model; ——, modified model.

adjusted such that y_- was equal to y_+, and the distribution of l was consistent with figure 15. This adjustment had little effect on the calculation of $\overline{v^2}$ and $\overline{uv}$, but improved the calculation of $\overline{U}$ and $\overline{u^2}$, to the extent where the double peak in the latter quantity is now reproduced qualitatively.

A second adjustment involved the introduction of a phase difference between u and v into the model. For an Oseen vortex, U and V are 90° out of phase, see (16), resulting in a zero value for $\overline{uv}$. Using spectral analysis, the data collected with the three-wire probe indicate that, at $x/d = 10$, U lags behind V by 95°–100° within the vortices for

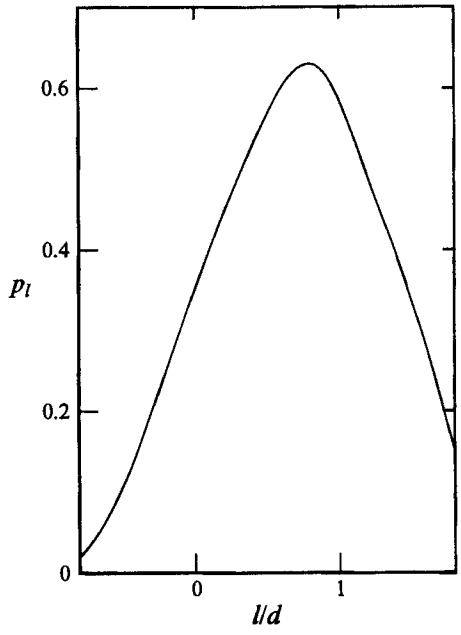

FIGURE 15. Probability density function of lateral separation between vortices of opposite sign.

$y/d > 0$, whereas U leads V by 80°–85° for $y/d < 0$. A phase shift ψ was therefore introduced into the computation of U, i.e. $U = U_0 - v_\theta \sin(\theta - \psi)$. The value of ψ was chosen to be 10° and its sign was the same as that of Γ_0; as a result, U lagged V by 100° for $\Gamma_0 < 0$ and led V by 80° for $\Gamma_0 > 0$, consistent with experimental observations. It was noted that the contribution of negative vortices to positive $\overline{uv}$ (below the centreline) is as large as 70–80%, whereas the contribution to negative $\overline{uv}$ (above the centreline) is of order 10–20%. This trend is reversed for positive vortices, suggesting that the concentration in the Reynolds shear stress resides mainly in the saddle region. Therefore, for $r < r_1$ the value of ψ is proportional to r/r_1 so that the phase shift mainly occurs for $r \geqslant r_1$. Note that the introduction of ψ only affects $\overline{uv}$ (there is no effect on $\overline{U}$, $\overline{u^2}$ and $\overline{v^2}$). Results obtained with the modified model are in reasonable agreement with measurements (figure 14).

The streamlines for part of the data corresponding to the modified model show good agreement with the conditional sectional streamlines (figure 16). Note that the streamlines do not spiral at the vortex centre because of the phase shift being introduced mainly for $r > r_1$. In Bisset *et al.*'s model, a phase shift was introduced mainly for $r < r_1$ and resulted in the streamlines spiralling out of vortex centres (their figure 14). In the near wake, streamlines may spiral into or out of individual vortex centres (figure 2), and the rate of occurrence for these two cases is nearly the same (Zhou & Antonia 1992*b*). Consequently, conditional streamlines are in general closed near the centre.

It should be noted that viscosity seems absent in the model since time is frozen and r_1 is constant, as in (2). This is different from some previous models, particularly for laminar wakes (e.g. Schaefer & Eskinazi 1959; Green & Gerrard 1991), which incorporate the effect of viscosity through the viscous diffusion term in (1). The viscous Oseen vortex, as described by (1), has a constant circulation but redistributes the vorticity as time varies. It is not apparent that this would be a good route to follow in our case, especially since our measurements indicate that the vortices maintain the

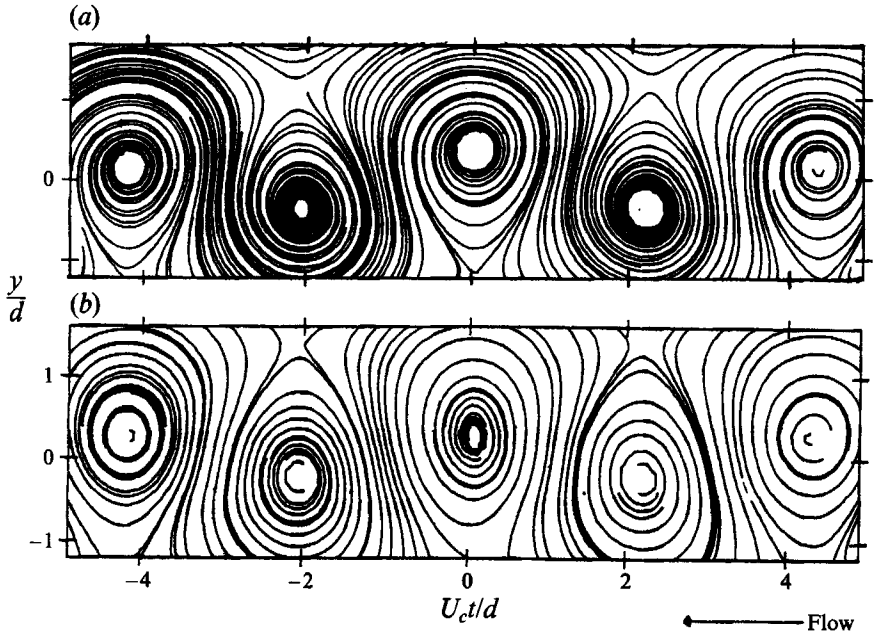

FIGURE 16. Comparison between sectional streamlines obtained from the modified model data (*a*) and from measurement (*b*) ($U_c/U_0 = 0.87$).

same relative distribution of vorticity (figure 6) as they travel downstream. Also note that the constancy of r_1, used in (2), is supported by the data in figure 10. In summary, the present model is more consistent with the measurements than the viscous Oseen vortex model.

Since the model is largely based on measurement and its basic building block is kinematically consistent with turbulent vortices, it provides a reasonable framework for interpreting experimental observations and perhaps gaining insight into mechanisms responsible for the production of Reynolds stresses. It seems clear that vortices are mainly responsible for $\bar{U}$ and the Reynolds normal stresses. The variation in the lateral location of the vortices reduces the mean velocity defect and increases substantially the magnitude of $\overline{u^2}$ near the centreline.

The present model is formed in the near wake ($x/d = 10$). At larger x/d, some modifications may be needed to account for flow development. For example, the opposing mode of vortices may become important as x/d increases (figure 12 indicates that the relative probability of duration between adjacent vortices of opposite sign has a larger spread at $x/d = 20$ than $x/d = 10$).

8. Conclusions

Turbulent vortices in the wake of a circular cylinder are detected by a method which includes vorticity and circulation criteria. The vorticity and circumferential velocity distributions which correspond to these detections are exponential in shape, similar to those for an Oseen vortex. Vorticity profiles normalized by the local peak vorticity are essentially unchanged in the range $x/d = 10$ to 60. Owing to the interaction between vortices of opposite sign, the longitudinal velocity distribution in the streamwise direction has its maximum at the centre of the vortex. This is consistent with earlier

measurements (Davies 1976; Zhou & Antonia 1992*a*) which indicated that the convection velocity of the vortex is greater than the local mean velocity, especially at small x/d.

An Oseen vortex model, which draws significantly from measurement, for example with respect to the strength, size and separations between vortices, reproduces the measured mean velocity and normal Reynolds stresses reasonably well. Reasonable agreement is also achieved for the Reynolds shear stress when a phase shift between u and v, similar to that observed in experiments, is included in the model.

The authors are grateful to Mr D. K. Bisset for his assistance with the programming, his suggestions and comments on this manuscript. The support of the Australian Research Council is gratefully acknowledged.

REFERENCES

ANTONIA, R. A. 1991 Organization in a turbulent near wake. *Fluid Dyn. Res.* **7**, 139–149.

BISSET, D. K., ANTONIA, R. A. & BROWNE, L. W. B. 1990 Spatial Organization of large structures in the turbulent far wake of a cylinder. *J. Fluid Mech.* **218**, 439–461.

BLOOR, M. S. & GERRARD, J. H. 1966 Measurements on turbulent vortices in a cylinder wake. *Proc. R. Soc. Lond.* A **294**, 319–342.

CANTWELL, B. & COLES, D. 1983 An experimental study of entrainment and transport in the turbulent near wake of a circular cylinder. *J. Fluid Mech.* **136**, 321–374.

CIMBALA, J. M., NAGIB, H. M. & ROSHKO, A. 1988 Large structure in the far wakes of two-dimensional bluff bodies. *J. Fluid Mech.* **190**, 265–298.

DAVIES, M. E. 1976 A comparison of the wake structure of a stationary and oscillating bluff body, using a conditional averaging technique. *J. Fluid Mech.* **75**, 209–231.

DRITSCHEL, D. 1988 Strain-induced vortex stripping. In *Mathematical Aspects of Vortex Dynamics* (ed. R. E. Caflisch), pp. 107–119. Soc. Ind. Appl. Maths.

GILL, P. E. & MURRAY, W. 1976 Minimization subject to bounds on the variations. *Rep.* NAC72. National Physical Laboratory.

GRANGER, R. A. 1985 *Fluid Mechanics*. New York: CBS College Pub.

GREEN, R. B. & GERRARD, J. H. 1991 An optical interferometric study of the wake of a bluff body. *J. Fluid Mech.* **226**, 219–242.

HOFFMANN, E. R. & JOUBERT, P. N. 1963 Turbulent line vortices. *J. Fluid Mech.* **16**, 395–411.

HUSSAIN, A. K. M. F. & HAYAKAWA, M. 1987 Education of large-scale organized structures in a turbulent plane wake. *J. Fluid Mech.* **180**, 193–229.

KIYA, M. & MATSUMURA, M. 1985 Turbulence structure in intermediate wake of a circular cylinder. *Bull. JSME* **28**, 2617–2624.

MCWILLIAMS, J. C. 1990 The vortices of two-dimensional turbulence, *J. Fluid Mech.* **219**, 361–385.

OKUDE, M. & MATSUI, T. 1987 Correspondence of velocity fluctuations to flow patterns in a Kármán vortex street at low Reynolds numbers. *Trans. Japan Soc. Aeron. Space Sci.* **30**, No. 88, 80–90.

OKUDE, M. & MATSUI, T. 1990 Vorticity distribution of vortex street in the wake of a circular cylinder. *Trans. Japan Soc. Aeron. Space Sci.* **33**, No. 99, 1–13.

OLER, J. W. & GOLDSCHMIDT, V. W. 1982 A vortex-street model of the flow in the similarity region of a two-dimensional free turbulent jet. *J. Fluid Mech.* **123**, 523–535.

ROBINSON, S. K. 1991 The kinematics of turbulent boundary layer structure. *NASA Tech. Memo.* 103859.

ROSHKO, A. 1954 On the drag and shedding frequency of two-dimensional bluff bodies. *NACA TN* 1191.

SAFFMAN, P. G. 1973 Structure of turbulent line vortices. *Phys. Fluids* **16**, 1181–1188.

SCHAEFER, J. W. & ESKINAZI, S. 1959 An analysis of the vortex street generated in a viscous fluid. *J. Fluid Mech.* **6**, 241–260.

SCHMIDT, D. W. & TILMANN, P. M. 1972 Über die Zirkulationsentwicklung in Nachläufen von Rundstäben. *Acustica* **27**, 14–22.

WEI, T. & SMITH, C. R. 1986 Secondary vortices in the wake of circular cylinders. *J. Fluid Mech.* **169**, 513–533.

ZHOU, Y. & ANTONIA, R. A. 1992*a* Convection velocity measurements in a cylinder wake. *Expts. Fluids* **13**, 63–70.

ZHOU, Y. & ANTONIA, R. A. 1992*b* A study of flow properties near critical points. *Proc. IUTAM Symposium Eddy Structure Identification in Free Turbulent Shear Flows, Poitiers*, pp. IX.2.1–IX.2.6.